

Acceleration feature points of unsteady shear flows

J. KASTEN¹⁾, J. REININGHAUS^{2,*)}, I. HOTZ^{3,*)}, H.-C. HEGE^{4,*)},
B. R. NOACK⁵⁾, G. DAVILLER⁶⁾, M. MORZYŃSKI⁷⁾

¹⁾*IVU Traffic Technologies AG, Berlin, Germany*
e-mail: webmaster@jens-kasten.de

**Formerly at Zuse Institute Berlin (ZIB), Berlin, Germany*

²⁾*IST Austria, Klosterneuburg, Austria*
e-mail: Jan.Reininghaus@ist.ac.at

³⁾*Linköping University, Norrköping, Sweden*
e-mail: Ingrid.Hotz@liu.com

⁴⁾*Zuse Institute Berlin (ZIB), Berlin, Germany*
e-mail: Hege@zib.de

⁵⁾*LIMSI-CNRS, Orsay, France*
and
Institut für Strömungsmechanik
Technische Universität Braunschweig, Germany
e-mail: Bernd.Noack@limsi.fr

⁶⁾*IMFT, CNRS, Toulouse, France*
e-mail: guillaume.daviller@imft.fr

⁷⁾*Poznań University of Technology, Poznań, Poland*
e-mail: Morzynski@stanton.ice.put.poznan.pl

A FRAMEWORK FOR EXTRACTING FEATURES IN 2D TRANSIENT FLOWS, based on the acceleration field to ensure Galilean invariance is proposed in this paper. The minima of the acceleration magnitude (a superset of acceleration zeros) are extracted and discriminated into vortices and saddle points, based on the spectral properties of the velocity Jacobian. The extraction of topological features is performed with purely combinatorial algorithms from discrete computational topology. The feature points are prioritized with persistence, as a physically meaningful importance measure. These feature points are tracked in time with a robust algorithm for tracking features. Thus, a space-time hierarchy of the minima is built and vortex merging events are detected. We apply the acceleration feature extraction strategy to three two-dimensional shear flows: (1) an incompressible periodic cylinder wake, (2) an incompressible planar mixing layer and (3) a weakly compressible planar jet. The vortex-like acceleration feature points are shown to be well aligned with acceleration zeros, maxima of the vorticity magnitude, minima of the pressure field and minima of λ_2 .

1. Introduction

COMPUTATIONAL FLUID DYNAMICS AND PARTICLE IMAGE VELOCIMETRY can provide highly resolved flow data in space and time. A first challenge is to quickly extract the important kinematic features from these data. Topological methods applied to snapshots are one of the first choices. Flow topology may provide information about the size of separation bubbles and vortices, about the length of a dead-water region, and about flow regions, which do not mix, just to name a few applications. Velocity snapshot topology provides invaluable insights into laminar or time-averaged flows [16, 32, 22, 26, 27] or, in general, into velocity fields with a distinguished frame of reference and a low feature density.

Such a topology is always based on the zeros of the velocity field and thus is intrinsically Galilean-variant, i.e., it depends on a chosen frame of reference. In an unsteady flow, a zero or a critical point at one instant is generally not a zero at another instant. The question of what critical point, 'connector' and other topological elements physically mean for an unsteady situation immediately arises and the answer is far from being clear.

In some cases, e.g., the flow over an obstacle, a naturally preferred body-fixed frame of reference is given. Here, Galilean invariance of the topology appears to be a purely academic requirement. In many cases, however, the proper frame of reference is far less obvious. In a wake or mixing layer, for instance, topology may resolve the initial vortex formation in a body-fixed frame of reference, but the convecting vortices do not give a rise to velocity zeros as they convect downstream. Now, the choice of the 'right' frame of reference is a subject of personal preferences.

A second challenge is that critical points are associated with the smallest structures present in the flow. In a fully turbulent flow, the average distance between fixed points is of the order of the Taylor scale [33, 34]. Under these conditions, critical points lose their meaning as 'markers' of large-scale coherent structures.

A third challenge is that every measured or simulated data naturally contains a small amount of noise. This noise complicates the extraction of feature points such as zeros. Therefore, important physical structures may be missed.

To address the first challenge, GOTO and VASSILICOS [9] used acceleration to define a set of feature points. They proposed to use zeros of the acceleration vector field (*zero acceleration points*) for the analysis of two-dimensional flows. The motivation for the definition of these zeros was to find a frame moving with vortices, such that the persistence of streamlines is maximized. However, extraction of physically meaningful zeros of the acceleration is a complex task, especially in the presence of noise.

In this paper, we propose acceleration feature points that comprise Goto’s ideas and solve challenges two and three. Acceleration feature points are: time-dependent counterparts of the fixed points of the velocity field topology. Their definition is based on three requirements: (1) choosing a Lagrangian viewpoint, (2) requiring Galilean invariance and (3) having standard velocity topology as limiting case for steady flows. It is shown that the minima of the acceleration magnitude, called *acceleration feature points*, fulfill these criteria. These points are Galilean-invariant and their physical meaning is inferred from the velocity Jacobian. They form a superset of the aforementioned by Goto and Vassilicos zero acceleration points. In contrast to their interesting work, our concept can be generalized to three-dimensional flows, and in particular to one-dimensional features.

Use of minima enables us to employ the powerful concept of scalar field topology and associated combinatorial extraction methods, which are robust against large noise levels in the data. The application of these methods enables the use of persistent homology [6]. It serves as (a) a filter for the robust extraction in the first step and (b) a spatial importance measure for acceleration feature points.

A subset of acceleration feature points can be interpreted as vortex cores. Within our combinatorial framework, we track these points over time. By a combination of persistence with the lifetime of the vortices, we are able to discriminate short-lived unimportant features from long-lived and dominant vortices. We therefore contribute to the vortex core distillation in three major points: (1) a robust extraction of the feature points in the presence of noise; (2) an efficient tracking of them over time; (3) a filtering strategy that is based on a hierarchy of the vortex cores and trajectories. The extraction and tracking process is based on a combinatorial framework [23, 24]. The resulting explicit representation of the vortex core lines enables a detailed analysis of the interacting structures in a flow field. In principle, an analogous feature extraction can be effected for saddles.

This paper is composed as follows. In Section 2, key elements of the analysis are defined for simple analytically defined flows. In Section 3, Galilean-invariant features are proposed. The algorithmic implementation of the feature extraction strategy is described in Section 4. The results are discussed in Section 5. Finally, Section 6 concludes the paper summarizing the findings and relating them to other topological analyses.

2. Illustrating shear flow example

In this section, a 2D incompressible flow is considered: the Stuart solution of the inviscid mixing layer [30]. This analytical example shows that lo-

cal minima of the total acceleration magnitude are good indicators of vortices and saddles. These results help to define of acceleration feature points as key elements of the feature extraction strategy that is discussed in the next section.

An incompressible mixing layer is described in a Cartesian coordinate system $\mathbf{x} = (x, y)$, where x and y represent the streamwise and transverse coordinate, respectively. The origin $\mathbf{0}$ is placed in one saddle. The velocity is denoted by $\mathbf{u} = (u, v)$, where u and v represent its x and y components, respectively. All quantities are normalized with half of the relative velocity difference and half of the vorticity thickness. Targeting a simple analytical example, we consider a streamwise periodic mixing layer with constant width, as described by the inviscid Stuart solution [30]:

$$(2.1a) \quad u = u_c + \frac{\sinh(y)}{\cosh(y) - 0.25 \cos(x - u_c t)},$$

$$(2.1b) \quad v = -0.25 \cdot \frac{\sin(x - t)}{\cosh(y) - 0.25 \cos(x - u_c t)},$$

where u_c represents the convection velocity.

The Stuart vortices are depicted in Fig. 1 as streamlines using planar line integral convolution (LIC) [3, 29]. The top picture represents Eq. (2.1) and shows the famous cat eyes in a periodic sequence of centers (vortices) and saddles for a vortex-fixed frame of reference ($u_c = 0$). The middle picture depicts the same structures but in a frame of reference moving to the left with the lower stream with velocity $(-0.7, 0)$, or, equivalently, the vortices moving to the right at $u_c = 0.7$. The centers and saddles are displaced towards the slower stream. The bottom picture illustrates the same flow with a frame of reference moving with velocity $(-1.2, 0)$, i.e., $u_c = 1.2$ in Eq. (2.1). Now, no zeros are observed. These figures recall the well-known fact, emphasized in many textbooks on fluid mechanics, that velocity field topology strongly depends on the frame of reference, i.e., is not Galilean-invariant. In case of the Stuart solution, one might argue that the frame of reference convecting with the structures is the most natural one. However, the convection velocity of a jet and many other flows depend on the streamwise position, i.e., generally no single natural frame of reference exists for topological considerations.

The saddles and centers of the Stuart solution for the vortex-fixed frame of reference ($u_c = 0$) are not only zeros of the velocity field but also zeros of the material acceleration field

$$(2.2) \quad \mathbf{a} = D_t \mathbf{u} = \partial_t \mathbf{u} + \mathbf{u} \cdot \nabla \mathbf{u}.$$

Here, ∂_t represents the partial derivative with respect to time, ∇ the nabla op-

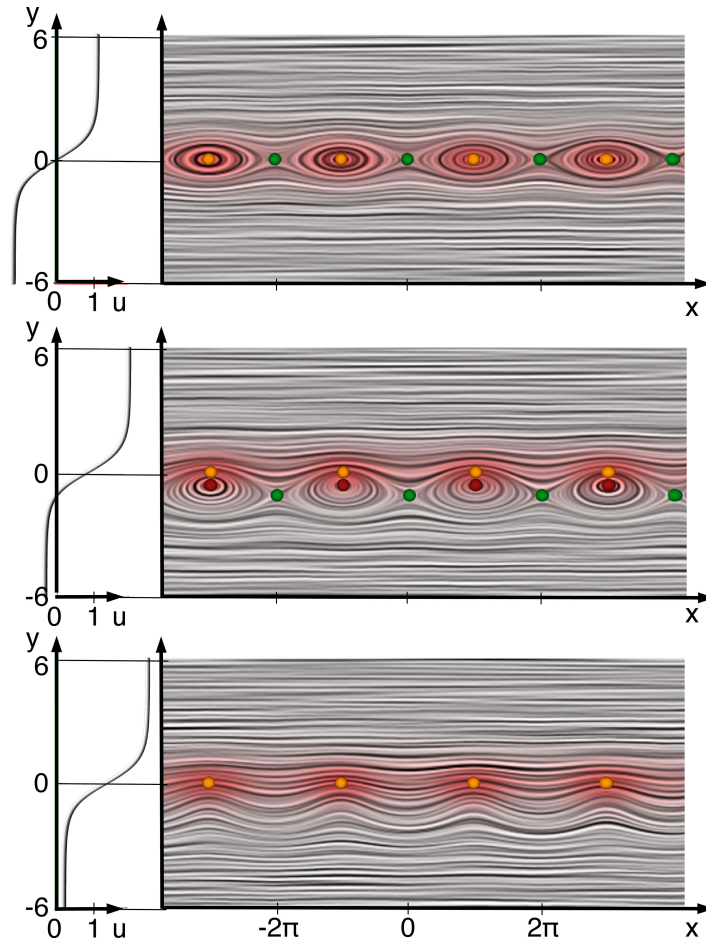


FIG. 1. Stuart vortices in various convecting frames. The mean velocity profile is shown at the left. The Stuart vortices are depicted by visualizing the instantaneous velocity field using line integral convolution. The coloring is determined by vorticity; more intense red corresponds to higher vorticity. The critical points of standard velocity field topology are displayed as red (centers) and green (saddles) spheres. The maxima of the vorticity are added as orange spheres.

erator and the dot \cdot is the tensor contraction. The acceleration zeros are derived from a Galilean-invariant field and do not depend on the chosen inertial frame of reference. Figure 2 illustrates the magnitude of the acceleration field as height field. The zeros of the acceleration field and the local minima of the acceleration magnitude (yellow spheres) coincide in this example. In general, the latter quantity is a superset of the first. However, the acceleration magnitude minima, enable to identify vortices and saddles in case of a non-uniform convection velocity.

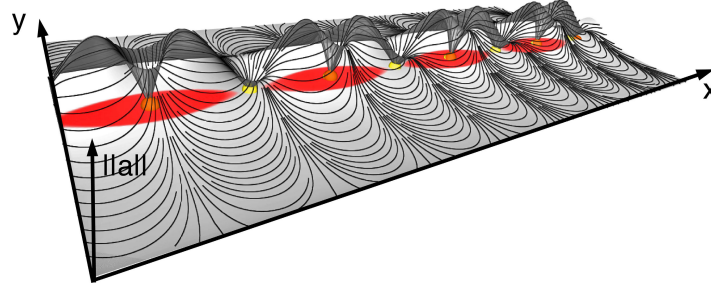


FIG. 2. The acceleration magnitude field of convecting Stuart vortices. The coloring at the bottom is determined by the vorticity. The height field shows the acceleration magnitude and the curves depict integral lines of the acceleration vector field. The yellow spheres highlight the acceleration minima, orange spheres vorticity maxima. Note that center-like acceleration minima and vorticity maxima coincide (orange spheres hide yellow spheres).

3. Acceleration feature points

In this section, the definition of the considered feature is introduced. A starting point is a critical review of the velocity snapshot topology. Topological analysis of velocity fields has been successfully applied to study flow fields with a distinguished frame of reference. However, its applicability is limited, as location and number of critical points depend on the frame of reference. The goal of the current study is to define of an alternative feature concept, which generalizes the snapshot topology in a local sense and overcomes the above-mentioned limitations. The feature point definition is motivated by the observations in the previous example and the following three requirements:

- (R1) Correspondence to velocity topology: A flow field is called steady, if there exists a distinguished frame of reference for which the vector field is stationary, i.e., it does not change in time. Such flow fields consist of *frozen* convective structures. In addition, they satisfy Taylor's hypothesis [31]. With respect to this distinguished frame of reference, critical points of the velocity field correspond to the position of vortex cores and saddles. This concept is not applicable to unsteady flow fields, since there is no such distinguished frame of reference. Aiming for a generalization of velocity topology, the newly defined feature points should coincide for steady flow fields with the zeros of the velocity field. This also means that the classification of the points as saddles or centers is preserved. Note that this requirement is not fulfilled by Haller's definition of a vortex [12]. Rotational invariant features cannot distinguish saddles and centers.
- (R2) Galilean invariance: A Galilean-invariant feature identifier reveals the same structures when changing the frame of reference.

- (R3) *Lagrangian viewpoint*: To guarantee a physically sensible feature identifier, we focus on particle motion. This Lagrangian viewpoint implies the focus on Galilean-invariant properties of fluid particles, but it does not include tracking finite-time fluid particle motion. This restricted Lagrangian viewpoint is consistent with the general notion of ‘Lagrangian coherent structures.’

The above requirements and the observations from Section 2 suggest to relate feature points to the material acceleration field. The particle acceleration \mathbf{a} is the total derivative of the flow field \mathbf{u} . In other words, the acceleration in a space-time point (\mathbf{x}, t) is given by Eq. (2.2).

DEFINITION. A minimum of the magnitude of the material acceleration $\|\mathbf{a}\|$ is called *acceleration feature point*. Such points can be classified on the basis of the Jacobian of the velocity field $\nabla\mathbf{u}$. A feature point is called *saddle-like* if its eigenvalues are real, and *center-like* if its eigenvalues are complex. A feature trajectory is defined by the temporal evolution of a minimum in the acceleration field.

In the following, this definition is shown to satisfy requirements R1 to R3. Let \mathbf{x}_0 be a zero of the steady velocity field $\mathbf{u}(\mathbf{x}_0, t) \equiv 0$. This implies that the material acceleration $\mathbf{a}|_{\mathbf{x}_0} = (\partial_t\mathbf{u} + \mathbf{u} \cdot \nabla\mathbf{u})|_{\mathbf{x}_0} = 0$ vanishes at \mathbf{x}_0 . Thus, the minima of the acceleration magnitude are a superset of acceleration zeros and these zeros are a superset of the critical points of the velocity field. Hence, acceleration feature points can be considered to be a generalization of the critical points of the velocity fields. Acceleration is a Galilean-invariant quantity. It is computed from the velocity using the material or Lagrangian derivative that links the Eulerian to the Lagrangian viewpoint [21]. Moreover, acceleration feature points satisfy all requirements R1 to R3.

The acceleration feature points can exhibit vortex-like as well as saddle-like behavior, depending on the eigenvalues of the velocity Jacobian. Real eigenvalues correspond to saddles, while a complex-conjugate eigenvalue pair indicates a vortex. Alternative synonymous discriminants have been proposed for 2D flows. For example, GOTO and VASSILICOS [9] showed that saddles are associated with sources of the material acceleration field while vortices correspond to sinks. One advantage of their definition is that it relies purely on the acceleration without a reference to the velocity Jacobian. BASDEVANT and PHILIPOVITCH [2] critically assessed the use of the ‘Weiss criterion’ as discriminant criterion.

Another perspective onto the acceleration minima is given by their relation to the pressure gradient via the incompressible Navier–Stokes equation:

$$(3.1) \quad \begin{aligned} \mathbf{a}(\mathbf{x}, t) &= -\frac{1}{\rho} \nabla p(\mathbf{x}, t) + \nu \Delta \mathbf{u}(\mathbf{x}, t), \\ 0 &= \nabla \cdot \mathbf{u}(\mathbf{x}, t), \end{aligned}$$

where p is the pressure of the flow field, ρ and ν are the kinematic viscosity and density of the fluid, respectively, and Δ is the spatial Laplacian operator. For ideal flows, the equations reduce to the Euler equation:

$$(3.2) \quad \begin{aligned} \mathbf{a}(\mathbf{x}, t) &= -\frac{1}{\rho} \nabla p(\mathbf{x}, t), \\ 0 &= \nabla \cdot \mathbf{u}(\mathbf{x}, t). \end{aligned}$$

Then, local extrema of the pressure field, which are zero points of the pressure gradient coincide with zeros of the acceleration field. In this case, the above defined acceleration feature points form a superset of local extrema of the pressure field, the minima of which are often associated with vortices.

4. Feature point extraction strategy

Besides the definition of physically meaningful feature points, the choice of a mathematical model for its description and a robust and efficient extraction algorithm is essential for practical applications. To be broadly applicable the mathematical framework should fulfill the following criteria:

- (C1) It should facilitate a robust and efficient extraction without subjective parameters to enable an unsupervised extraction of the structures.
- (C2) It should allow to generate a feature hierarchy based on an intrinsic filtering mechanism. This eases the interpretation of the results and becomes necessary as soon as one moves on from simple showcases or when the data exhibit high feature densities.
- (C3) It should allow for tracking of features over time, based on neighborhood relations.

The above defined *acceleration feature points* can be considered as part of the scalar field topology of the acceleration field just like extremal points of the acceleration magnitude. This interpretation gives access to powerful algorithmic tools developed for extracting and tracking topological structures in scalar fields. Our feature extraction pipeline consists of three steps: (1) spatial feature extraction resulting in isolated feature points; (2) temporal tracking of these points; and (3) spatio-temporal filtering of the resulting structures, cf. Fig. 3. In the following, we will briefly describe the methods used for the three steps in the extraction pipeline. We restrict the description to two-dimensional case since this corresponds to our setting. All these concepts can be generalized to higher dimensions. However, the cases to consider will become more complex.

(1) *Combinatorial extraction of two-dimensional scalar field topology.* The algorithm chosen for this paper is based on *discrete Morse theory* [7]. A short

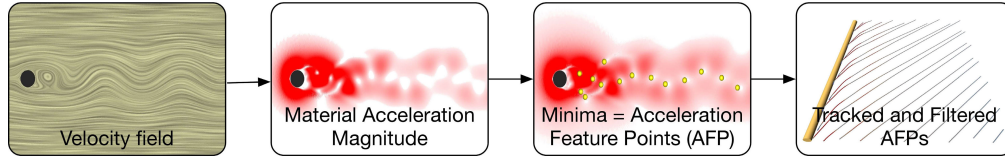


FIG. 3. Pipeline of the proposed approach: After computing the acceleration magnitude field from the velocity, its minima are extracted, which are referred to as *acceleration feature points* (AFPs). These AFPs are tracked over time and prioritized by a spatio-temporal importance measure. The importance measure combines a spatial strength and the lifetime of the feature.

introduction to this theory is given in Appendix A of this paper. It is purely combinatorial and guarantees topological consistency of the extracted structures [23]. The robustness of the algorithm and lack of any algorithmic parameter allow an unsupervised extraction of structures. This guarantees the applicability of the methods to large data sets without tedious adaptations.

(2) *Temporal feature development.* To get an understanding of the temporal evolution of acceleration feature points, the minima are tracked over time. We use here a topological tracking also referred to as *combinatorial feature flow fields* (CFFF), as proposed in [24]. The basic idea of this tracking algorithm is to construct a discrete gradient field in space-time, describing the development of the acceleration minima, such that tracking of those minima results in an integration of the discrete gradient field [15]. The result of this tracking is a set of temporal feature lines with explicit mergers and splits, which allows us to extract the mergers that occur for vortex core lines in a two-dimensional setting.

(3) *Generating a feature hierarchy for the tracked acceleration feature points.* One way to approach the problem of a high feature density are statistical methods. Another way, pursued in this work, is to facilitate an importance measure to build a feature hierarchy. A commonly used importance measure for critical points in context of scalar field topology is *persistent homology* [6]. Persistence measures the stability of critical points with respect to small changes in the data, e.g. introduced by noise.

More specifically, it is based on the notion of the persistence of components in the sublevel sets of a scalar function. Sublevel sets of a scalar function are defined as the set of all points having a scalar value below a certain threshold. By increasing this threshold new components are generated in minima or saddle points of the function, while they disappear in saddles or maxima. In this way critical points are paired in an hierarchical manner (minimum-saddle or saddle-maximum) and are assigned a persistence value. These pairs can then be cancelled to simplify the data in a well-defined and controlled way with strict error measures. In our setting, this means that every acceleration minima is assigned an importance value. Note that critical points that are paired by persistence

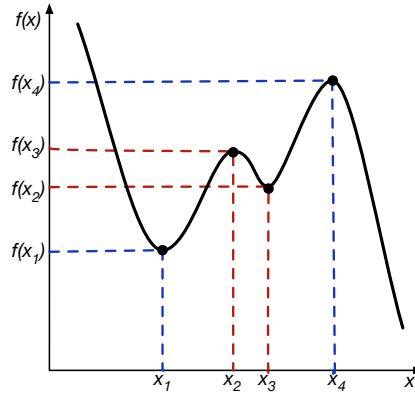


FIG. 4. The employed spatial feature importance is given by the persistent homology of the critical points. It measures how strong a minimum is, compared to its neighbors. This is achieved by correctly pairing critical points and quantifying their height difference. The image shows such a pairing, e.g., the critical points at x_2 and x_3 . As an example, the persistence associated with x_1 is $f(x_2) - f(x_1)$. This is, loosely speaking, the lowest height one needs to climb to get to the next critical point.

are not necessarily adjacent. For a simple example illustrating the concept of persistent homology, we refer the reader to Fig. 4.

From this importance measure for critical points we derive a spatio-temporal measure for the features by integrating persistence along the feature line, e.g., by accumulating all persistence values along the line. This measure takes the feature strength as well as its lifetime into account.

5. Results

Three canonical free shear flows are investigated: the flow around circular cylinder, a planar mixing layer, and a planar jet. These well-studied configurations represent different levels of spatio-temporal complexity from the periodic wake to the broadband dynamics and vortex pairing of the mixing layer and jet. The first two flows share a pronounced uniform far-wake convection velocity, while the jet structures move slower with streamwise distance.

The 2D cylinder wake has been a subject of numerous topological analyses. The steady flow is symmetric and has a single separation point up to a Reynolds number of $Re = 4$ (based on diameter) [35]. At larger Reynolds numbers, a symmetric vortex pair emerges. It should be noted that this topological bifurcation results from a continuous change of a stable steady solution and is not associated with any dynamical bifurcation. This vortex pair becomes unstable in a supercritical Hopf bifurcation at $Re = 47$ [28, 18]. The near-wake topology of the resulting periodic wake was studied in detail by BRØNS *et al.* [1]. Their study

reveals rich set of topological configurations and their temporal transitions, all in a body-fixed frame of reference. Additionally, the far wake contains no velocity zeros according to their study. Yet, the topology assumes a nearly periodic pattern in streamwise direction if the frame of reference moves with the vortices. Thus, the topology of the near and far-wake is best elucidated in frame of reference which moves with the vortices with vanishing speed in the near wake to about 85% of the oncoming velocity further downstream. The need for different frames of references indicates a challenge to Galilean variant features.

A pronounced topological feature of the Kelvin-Helmholtz instability of shear flows is the so-called ‘cat’s eye’ where the saddle points connect via heteroclinic orbits and thus strap the circulating particles inside the vortex [13, 30]. ‘Cat’s eyes’ can only be observed in a suitable frame of reference, as demonstrated in Section 2. Vortex pairing gives a rise to a far more complicated topology. For planar jets, convection velocities ranging from zero in the far-field to about 65% of the exit velocity are reported.

In contrast to the velocity field, the acceleration field is Galilean invariant and the equilibrium points of the latter is a superset of the velocity zeros (in any inertial frame of reference). Focus of this study is placed on the vortex skeleton as identified by the Galilean-invariant acceleration feature points (AFPs). All flows are described in a Cartesian coordinate system $\mathbf{x} = (x, y)$, of which the abscissa x points in streamwise direction and y in transversal direction. The origin is located in the source of the shear flow, i.e. center of the cylinder for the wake, center of the inflow for the mixing layer and center of the orifice for the jet.

The velocity $\mathbf{u} = (u, v)$ is expressed in the same system, u and v being the x - and y -components of the velocity. The time is denoted by t , the pressure by p and the material acceleration by \mathbf{a} . All quantities are non-dimensionalized with a characteristic length-scale L , a characteristic velocity U and the density of the fluid ρ . L denotes the cylinder diameter for the wake, the vorticity thickness for the mixing layer and the width of the orifice for the planar jet. U corresponds to the oncoming flow for the wake, to the velocity of the upper (faster) stream for the mixing layer, and to the maximum velocity at the orifice for the jet.

This section of the paper is organized as follows. Feature extraction results of the cylinder wake, the mixing layer, and the planar jet are present in Sections 5.1, 5.2 and 5.3, respectively. Pars pro toto, we perform a statistical analysis for the wake features, investigate the vortex merging of the mixing layer, and employ the persistence-filter of AFPs for the jet.

5.1. Cylinder wake

A starting point is a benchmark problem for the data visualization community: periodic vortex shedding behind a circular cylinder. The Reynolds number

is set to 100, which is well above the critical value of 47 for vortex shedding [36, 14] and well below the critical value of around 180 for transition-related instabilities [37, 35]. The flow is simulated with a finite element method solver with third-order accuracy in space and time, like in [18]. The rectangular computational domain $(x, y) \in [-10, 30] \times [-15, 15]$ without the disk $K_{1/2}(0)$ for the cylinder is discretized by 277576 triangular elements. The numerical time step for implicit time integration is 0.1, which also corresponds to the sampling frequency for the snapshots.

Figure 5 shows five vorticity related quantities of a cylinder wake snapshot. The vorticity field depicts the separating shear-layers rolling up in a staggered array of alternating vortices. The yellow balls mark the extrema, revealing the known fact that the ratio between the transverse of vortex displacement and the wavelength slightly increases downstream with vortex diffusion. The second subfigure shows the Okubo-Weiss parameter $Q = \|\mathbf{S}^-\|^2 - \|\mathbf{S}^+\|^2$ marking the maxima with balls. This parameter employs the velocity Jacobian $\nabla \mathbf{u}$ and compares the norm of the symmetric shear tensor $\mathbf{S}^+ = \frac{1}{2}[\nabla \mathbf{u} + (\nabla \mathbf{u})^t]$ with the norm of the antisymmetric one $\mathbf{S}^- = \frac{1}{2}[\nabla \mathbf{u} - (\nabla \mathbf{u})^t]$. In the center of a radially symmetric vortex, $Q = \|\omega\|^2 > 0$, since $\|\mathbf{S}^+\|$ vanishes and $\|\mathbf{S}^-\|$ becomes the norm of the vorticity $\|\omega\|$. At a saddle point $Q = -\|\mathbf{S}^+\|^2 < 0$. Hence, maxima of Q can be associated with vortex centers and minima with saddles. The third subfigure shows λ_2 . Its extrema are marked by balls and indicate vortex centers. Q and λ_2 are generally considered to provide synonymous information. The absolute value of the imaginary part of the eigenvalues of the Jacobian $\nabla \mathbf{u}$ is shown in the fourth subfigure. This quantity characterizes the angular frequency of revolution of a neighboring particles. Hence, its maxima marked by yellow balls indicate vortex centers. Finally, the magnitude of the material acceleration field is depicted in the fifth (bottom) subfigure. The minima (zeros) mark both vortex centers and saddles, i.e., twice as many points in the vortex street. These two features are distinguished based on the velocity Jacobian: two positive eigenvalues of the velocity Jacobian are associated with a saddle, a complex conjugate pair with a vortex.

In the vortex street, all five vortex criteria provide nearly identical locations. In the boundary-layer and in the near-wake of the cylinder there are pronounced differences. Mathematically, the vortex criteria rely on quite different formulae. They cannot be expected to exactly coincide except for pronounced flow features, e.g., axis-symmetric vortices. In addition, the cylinder boundary introduces a singular line $\mathbf{u} = \mathbf{0}$, thus amplifying the differences between the vortex criteria.

Figure 6 shows the spatial-temporal vortex evolution, based on the tracked acceleration feature points. In the far-wake, a uniformly convecting von Kármán vortex street is observed. In the near-wake, the convection speed is significantly

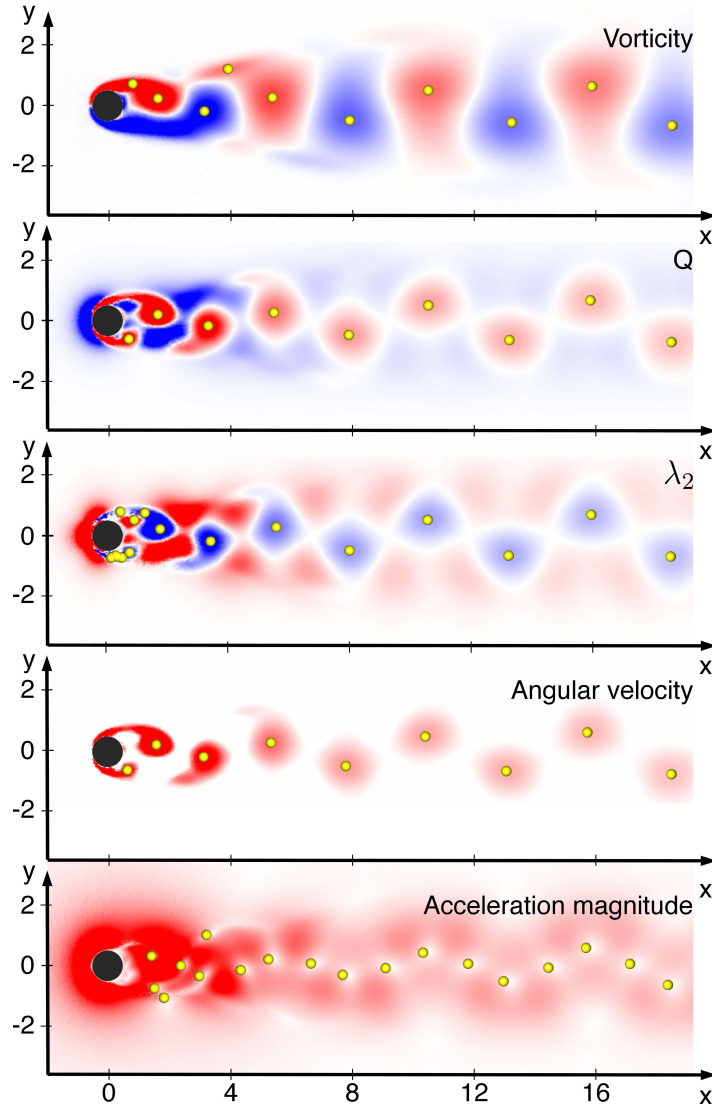


FIG. 5. Visualization of a cylinder wake snapshot. Five vorticity-related quantities are depicted by color maps (red: positive values, blue: negative, gray: zero): (1) vorticity, (2) Okubo–Weiss parameter, (3) λ_2 , (4) absolute value of the imaginary part of the eigenvalues of the velocity Jacobian, which corresponds to the angular velocity and (5) material acceleration magnitude. The yellow spheres depict the extremal points typically used as features for the respective quantity.

slower. This aspect is highlighted in Fig. 7 (first subfigure). The streamwise velocity of each vortex u_v is a monotonically increasing function from 0.03 to about 0.85. The asymptote corresponds to the value provided in [35]. The transverse

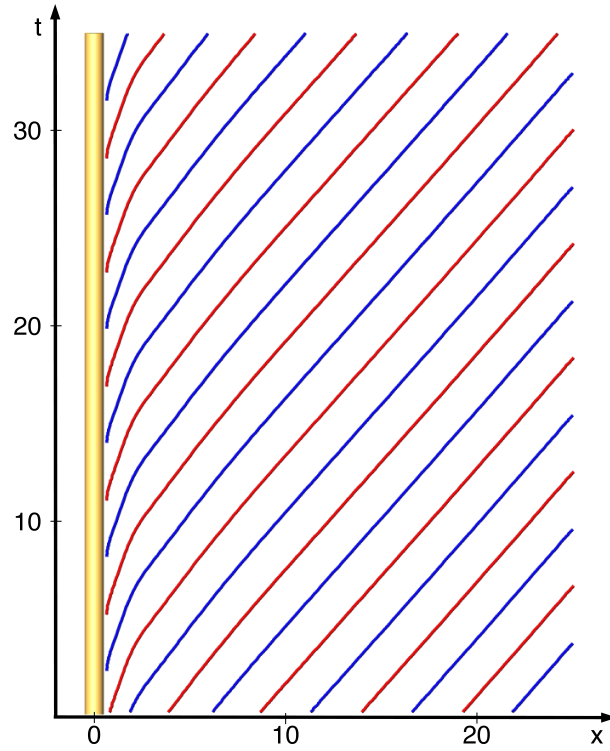


FIG. 6. Tracked vortices of the cylinder wake in an xt view. Red (blue) marks positive (negative) rotation of the vortices.

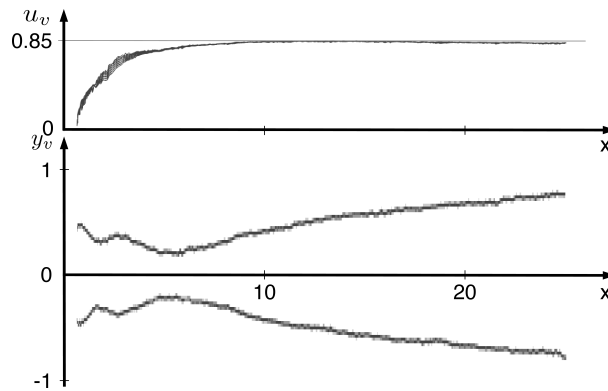


FIG. 7. Plots of the streamwise velocity component u_v (top) and the transverse displacement y_v (bottom) along tracked vortices. Note that each figure contains the history of many vortex evolutions from roll-up to convection out of the domain. Hence, several lines can be seen in each curve.

spreading of the vortex street, observed Fig. 5, is quantified in the following subfigure with the transverse location y_v .

It should be noted that tracked acceleration feature points can be seen as markers of coherent structures. The acceleration-based framework provides convenient means for determining convection velocities and evolution of spatial extensions. The following investigations of the mixing layer and the jet flow emphasize this aspect.

5.2. Mixing layer

The second investigated shear flow is a mixing-layer with a velocity ratio between upper and lower stream of 3:1, following earlier investigations of the authors [5, 20, 19]. The inflow is described by a tanh profile with a stochastic perturbation. The Reynolds number based on maximum velocity and vorticity thickness is 500. The flow is computed with a compact finite-difference scheme of sixth order accuracy in space and third order accuracy in time. The computational domain $(x, y) \in [0, 140] \times [-28, 28]$ is discretized on a 960×384 grid. The sampling time for the employed snapshots is $\Delta t = 0.05$ corresponding to 1/10 of the computational time step. Linear interpolation has been used for the visualization, whenever it was require.

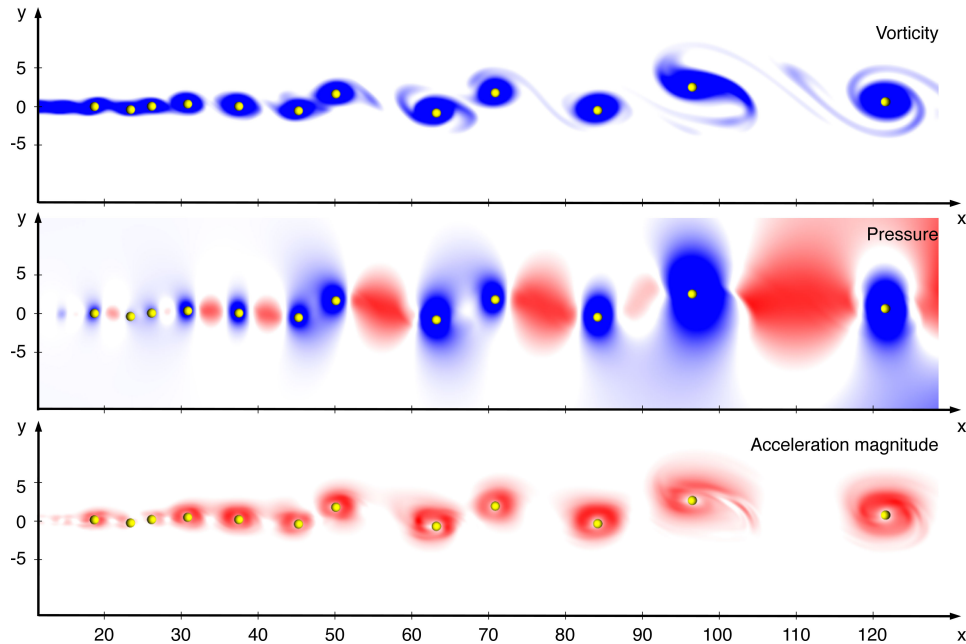


FIG. 8. Visualization of a mixing layer snapshot. Comparison of vorticity (top), pressure (middle) and acceleration (bottom). The color scheme is blue (red) for negative (positive) values. The yellow spheres represent pronounced vortex acceleration feature points.

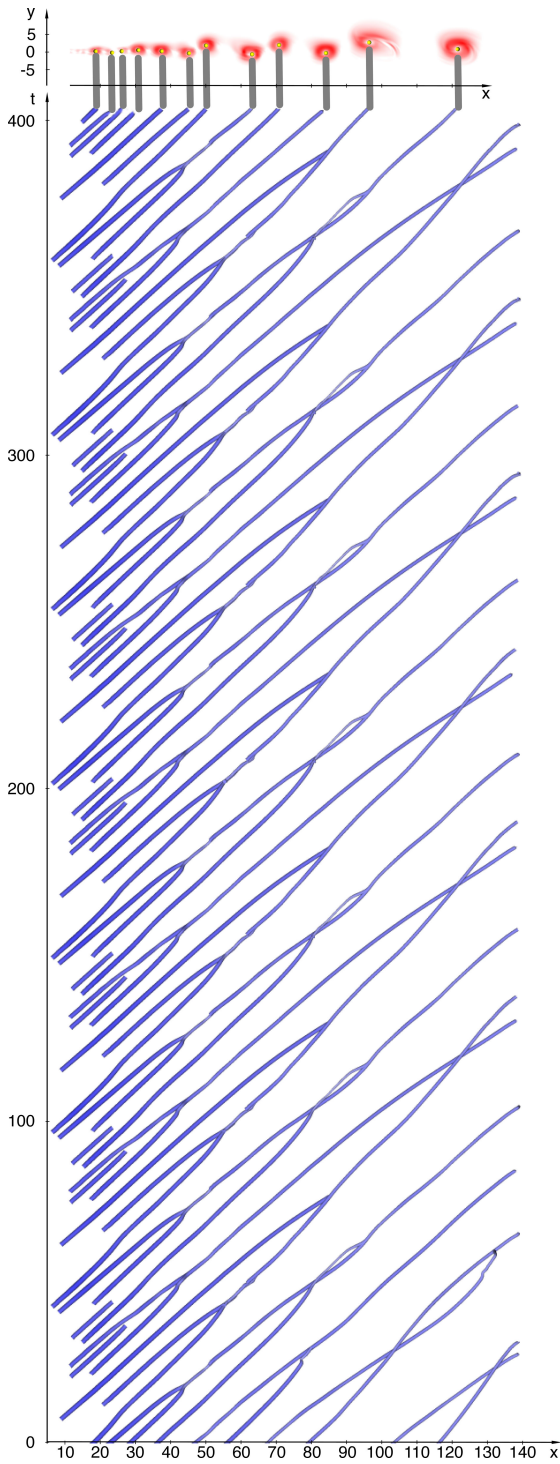


FIG. 9. Spatio-temporal evolution of vortices in the mixing-layer. The top part of the figure shows the acceleration magnitude field and LEPs at the final time considered. The bottom of the figure marks the tracked acceleration feature points over approximately five downwash times. Numerous vortex merging events can be identified. The size and coloring of the vortex skeleton is determined by vorticity, more intense blue corresponds to lower vorticity. Note that vorticity is negative everywhere.

In contrast to the space- and time-periodic Stuart solution, the mixing layer generally shows several vortex pairing events. In Fig. 8, the distance between vortex acceleration feature points (marked by balls) are seen to increase in streamwise direction as a result of vortex merging. Furthermore, the locations of the acceleration feature points nicely correlate with the local maxima of the vorticity (top), the local minima of the pressure (middle) and the local minima of the magnitude of the material acceleration (bottom). The correlation between vorticity maxima and pressure minima in free shear flows is well documented in the literature. The correlation between pressure and acceleration magnitude minima may be inferred from the non-dimensionalized Euler equation $\mathbf{a} = -\nabla p$, governing the predominantly inviscid dynamics of the mixing layer. A pressure minimum (or maximum) implies $\nabla p = 0$ and thus $\mathbf{a} = 0$.

The vortex merging events are shown in Fig. 9. Upstream, many Kelvin–Helmholtz vortices are formed. In streamwise direction, numerous vortex merging can be identified. The downstream vortices result from up to four successive vortex mergers in the shown domain. Not all crossings of x, t -curves mark mergers since vortex pairs may rotate around their center before eventually merging. The figure strongly suggests a nearly constant streamwise convection velocity, as expected from the literature results and contrary to the cylinder wake dynamics.

5.3. Planar jet

Finally, the spatio-temporal evolution of the planar jet is investigated. Like the mixing layer, the jet shows a number of vortex mergers leading to a reduction of the characteristic frequency. An additional complexity is the fact that the convection velocity is not constant but decreases in streamwise direction.

All quantities are normalized with the jet width D_j and the maximum jet velocity U_j . The flow is a weakly compressible isothermal 2D jet with a Mach number of $Ma_j = 0.1$ and a Reynolds number of $Re_j = D_j U_j / \nu_\infty = 500$. The inflow velocity profile is given by a hyperbolic tangent profile like in [8]:

$$u(r) = U_\infty + \frac{(U_j - U_\infty)}{2} \left[1 - \tanh \left[b \left(\frac{r}{r_0} - \frac{r_0}{r} \right) \right] \right].$$

Here, a uniform 1% co-flow $U_\infty = 0.01 U_j$ is added to avoid vortices with arbitrarily long residence time in the computational domain. The slope of the tanh profile is characterized by $b = r_o / 4\delta_\theta$ and the momentum thickness of the shear layer is $\delta_\theta = 0.05 r_o$. The initial mean temperature was calculated with the Crocco–Busemann relation, and the mean initial pressure was constant.

The natural transition to unsteadiness is aided by adding disturbances into a region during the early jet development near the inflow boundary $x_o = -0.5$:

$$(5.1) \quad v(x, y) = v(x, y) + \alpha U_c e^{-\frac{(x-x_o)^2}{\lambda_x^2}} (f_1(y) + f_2(y)).$$

Here,

$$(5.2) \quad f_1(y) = \epsilon_1 e^{-\frac{(y-y_1)^2}{\lambda_y^2}}, \quad f_2(y) = \epsilon_2 e^{-\frac{(y-y_2)^2}{\lambda_y^2}},$$

where $U_c = 0.5$, $\alpha = 0.008$, $y_1 = 0.5$, $y_2 = -0.5$, $\lambda_x = 0.1$, $\lambda_y = 0.1$ and $-1 \leq \epsilon_1, \epsilon_2 \leq 1$ are random numbers.

The flow is defined in a rectangular domain $(x, y) \in [0, 20] \times [-7, 7]$. The adjacent sponge zone extends to $[-1.5, 25] \times [-10, 10]$. The whole domain is discretized on a non-uniform Cartesian grid with 2449 points in x -direction and 598 points in y -direction. The compressible Navier–Stokes equation is solved by means of a $(2, 4)$ conservative finite-difference scheme, based on MacCormack’s predictor-corrector method [10] with block-decomposition and MPI parallelization. The system may be closed by the thermodynamic relations for an ideal gas. Details of the equations, boundary conditions and solver can be found in [4].

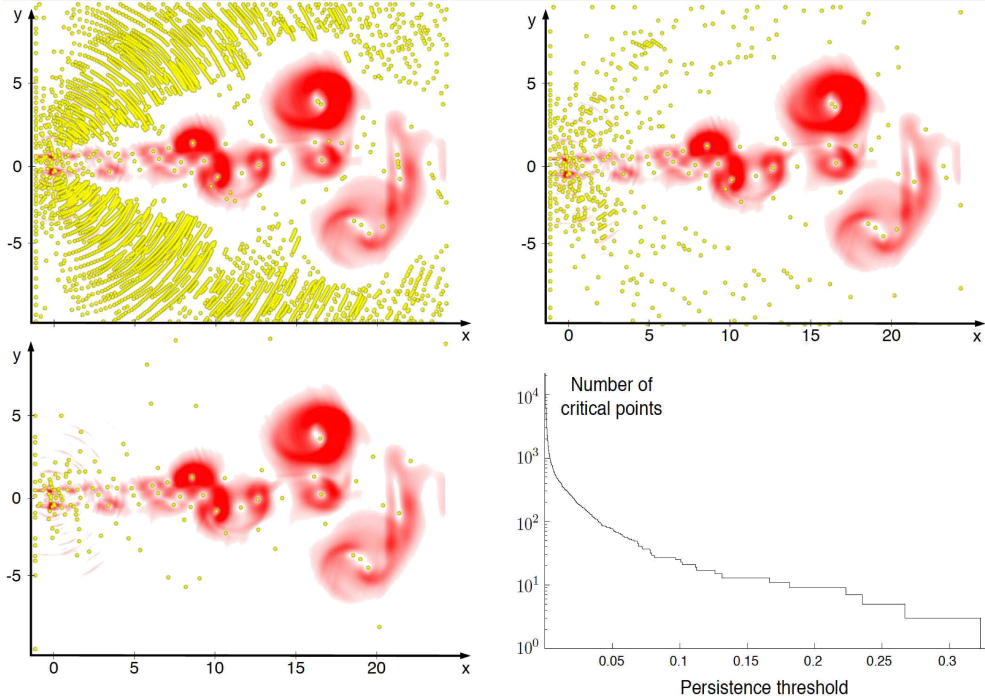


FIG. 10. Persistence-based visualization of a jet snapshot. *Top left to bottom left*: visualization of the snapshot for persistence threshold levels of 0% (top left), 0.5% (top right) and 2% (bottom left) of the maximum. The color field depicts the acceleration magnitude with a color map that ranges from white (zero) to red (positive). The yellow balls represent acceleration feature points filtered by their persistent homology with respect to the specified threshold levels. *Bottom right*: persistence distribution. The number of critical points after persistence-based filtering is plotted against the persistence threshold level.

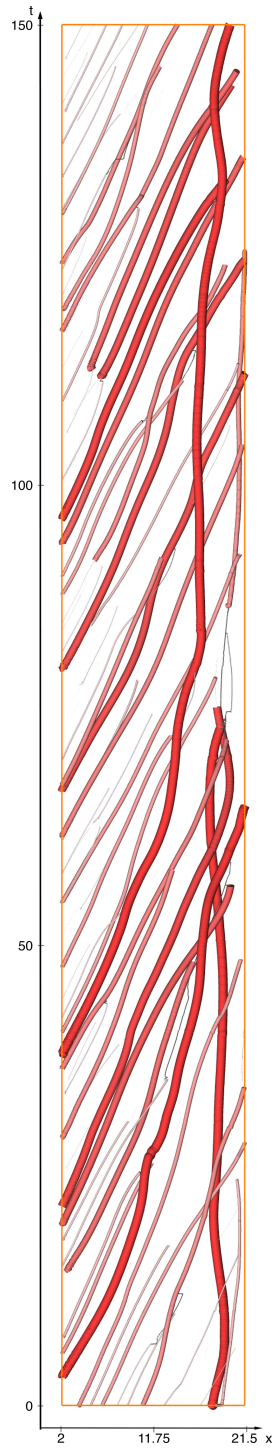


FIG. 11. Spatio-temporal evolution of the vortex skeleton of the jet. The size and coloring of the vortex lines are determined by our spatio-temporal importance measure. The links between the individual vortices are shown as white gray lines.

A stochastic inflow perturbation gives a rise to small acoustic waves. These small acoustic perturbations provide an excellent test-case demonstrating the need and performance of persistence-based filtering. Figure 10 depicts a jet snapshot. Most of the acceleration feature points are associated with low-amplitude sound waves from the random inlet perturbation (top figure). These acceleration feature points may be filtered out, ignoring those with low persistence (middle and bottom figures). The bottom figure only shows features associated with incompressible dynamics.

The spatio-temporal evolution of the vortex skeleton of the jet is visualized in Fig. 11 in a similar manner as the wake (Fig. 6) and the mixing-layer (Fig. 9). Clearly, vortex merging events and a streamwise decreasing convection velocity can be identified. In particular, some strong vortices remain for a long time near the exit. A three-dimensional close-up view is shown in Fig. 12.

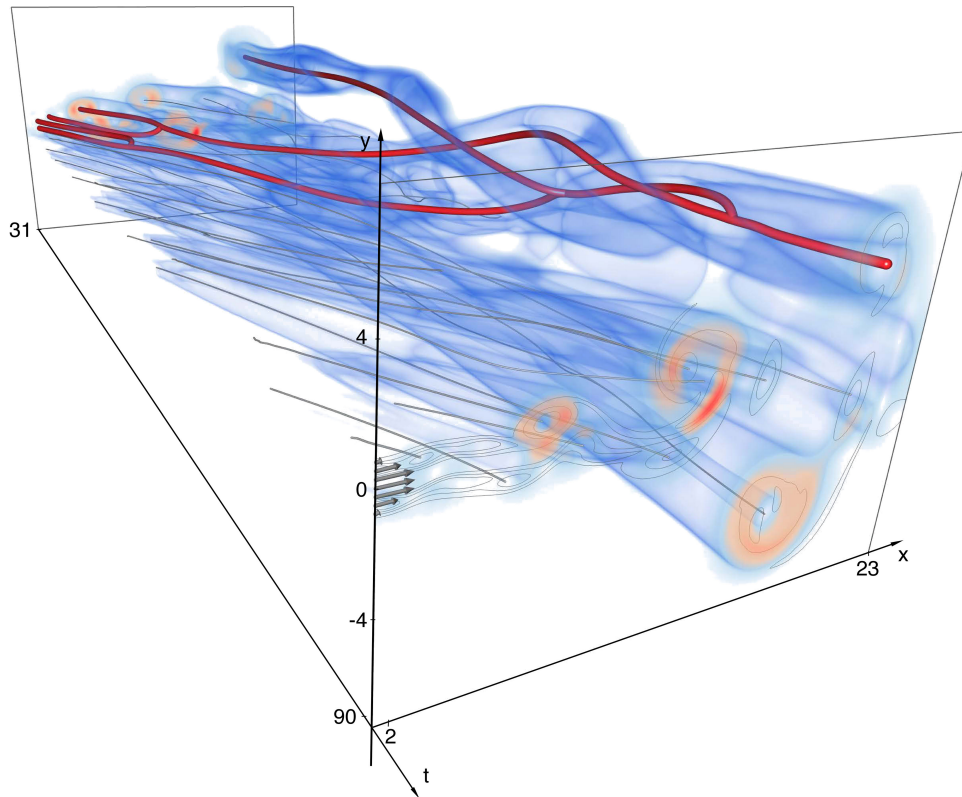


FIG. 12. Close-up view of the vortex skeleton of the jet flow. The gray lines depict the extracted and filtered vortex cores. A few lines are visually highlighted by red coloring; they show a pronounced vortex merging event and the origin of the merged vortices. The acceleration is visualized by the blue volume rendering and the color coding in the front and back planes. For comparison, iso-lines of the vorticity are added to the front plane.

6. Conclusions

We have proposed a novel feature extraction strategy for unsteady 2D flows. This strategy departs in important aspects from topology extraction of the instantaneous velocity field, starting from the velocity zeros. Instead of the velocity, the material acceleration field is analyzed, following [9]. Secondly, instead of acceleration zeros, the minima of the acceleration magnitude are identified. Thirdly, the acceleration feature points are tracked in time. Finally, a mathematically rigorous spatiotemporal hierarchy of the tracked minima is defined.

The acceleration feature points define topological elements of an unsteady flow with a number of discriminating features:

1. For steady flows, the acceleration feature points are a natural generalization of the critical points of vector field topology. Each critical point is an acceleration feature point. This implication may not hold generally in the other direction.
2. A critical point of a steady flow field remains an acceleration feature point in any inertial frame of reference. In other words, the acceleration feature points cannot vanish or be distorted by a uniform convection of a 'frozen' flow field (Taylor hypothesis).
3. The acceleration feature points are independent of the inertial frame of reference, i.e., they are Galilean-invariant. This property is a trivial consequence of the material acceleration field as observable.
4. The concept of acceleration feature points is parameter-free. No integration windows, nor threshold criteria, etc. are needed. Note that the persistence level is not a free parameter, as it defines a feature hierarchy.
5. Acceleration is correlated with pressure by neglecting the viscous term. Suppose the pressure field has a minimum (in a vortex) or maximum (near a saddle point). Then, the pressure gradient vanishes and the Euler equation yields a vanishing material acceleration (implying trivially also a magnitude minimum).
6. The persistence measure introduces a rigorous hierarchy of acceleration feature points based on spatial characteristics, without the need of temporal filtering.
7. With the tracking of the acceleration feature points, the temporally integrated persistence emphasizes long-lived structures.

In short, identification of acceleration feature points naturally generalizes identification of critical points and exhibits new desirable or even necessary properties for a meaningful flow analysis.

Our framework follows VASSILICOS and GOTO [9] in employing the Galilean-invariant material acceleration field as opposed to the velocity field. However, Vassilicos determined the zeros of this field, while our acceleration feature points are based on the more general notion of magnitude minima. This enables a robust, computationally inexpensive, derivative-free feature extraction that is capable of coping with large noise levels in the data. Furthermore, using minima instead of zeros allows for a natural extension to three-dimensional flows. The concept of acceleration feature points follows Haller in the search of a Lagrangian viewpoint of a Galilean invariant definition of saddles [11] and vortices [12], however it provides a simple aggregate definition for both features. The hierarchy of the acceleration feature points can be determined from a single snapshot, i.e., no back and forward integration of fluid particles is required.

The framework has been applied to three free shear flows: periodic vortex shedding of a cylinder wake, a mixing layer with a small range of dominant frequencies, and a planar jet with broadband dynamics. In all cases, the acceleration feature points are cleanly distilled from the numerical data and they enable additional insights. For the wake flow, vortex-based statistics are possible, e.g., for determining the streamwise convection velocity. For the mixing layer, vortex merging events are specified in time and space. And for the jet, persistence is used to separate between aeroacoustic and hydrodynamic equilibrium points.

In the numerical analyses, only vortices have been considered. Here, vortices are acceleration feature points with imaginary eigenvalues of the velocity Jacobian. Analogously, saddles can be defined as acceleration feature points with real eigenvalues of this Jacobian matrix. Thus, the concept of acceleration feature points represents a unifying framework for the main generic features of 2D flows. Furthermore, it offers a computationally inexpensive alternative to the concept of the finite-time Lyapunov exponent [11]. We actively pursue a 3D generalization of the proposed feature extraction.

Acknowledgments

The authors acknowledge funding of the German Research Foundation (DFG) via the Collaborative Research Center (SFB 557) “Control of Complex Turbulent Shear Flows” and the Emmy Noether Program. Further funding was provided by the Zuse Institute Berlin (ZIB), the DFG-CNRS research group “Noise Generation in Turbulent Flows” (2003–2010), the Chaire d’Excellence ‘Closed-loop control of turbulent shear flows using reduced-order models’ (TUCOROM) of the French Agence Nationale de la Recherche (ANR), and the European Social Fund (ESF App. No. 100098251). This work has been funded by Polish National Centre of Science under research grant no. 2011/01/B/ST8/07264 “Novel Method of Physical Modal Basis Generation for Reduced Order Flow Models”.

We thank the Ambrosys Ltd. Society for Complex Systems Management and the Bernd R. Noack Cybernetics Foundation for additional support. A part of this work was performed using HPC resources from GENCI-[CCRT/CINES/IDRIS] supported by the Grant 2011-[x2011020912]. We appreciate valuable stimulating discussions with William K. George, Michael Schlegel, Gilead Tadmor, Vassilis Theofilis, and Christos Vassilicos as well as the local TUCOROM team: Jean-Paul Bonnet, Pierre Comte (deceased), Laurent Cordier, Joël Delville (deceased), and Andreas Spohn. The figures have been created with Amira, a system for advanced visual data analysis (<http://amira.zib.de>).

Appendix. Introduction to Discrete Morse theory

This section gives a short introduction to Discrete Morse theory, which is the basis of our feature extraction method. Due to the complexity of this topic we will only give a strongly simplified informal summary of some basic ideas for a two-dimensional case.

Morse functions. Morse theory [17] investigates the relationship of the critical points of a smooth function f given on a domain Ω and the topology of the domain. *Critical points* of f are points where the gradient of f is zero. They can be classified with respect to the sign of the eigenvalues of the Hessian of f . In two-dimensional case these are *minima*, *saddles*, and of *maxima*. If the determinant of the Hessian at a critical point is nonzero, then it is called a *non-degenerate*. If all critical points of f are non-degenerate, then f is called a *Morse function*. The Morse theorem gives now a relation between the critical points of the function f and the topology of the domain Ω and allows to define critical points in a purely topological fashion. Morse theory also defines the admissible set of critical points of a function defined on Ω which is very useful for computational purposes.

Morse-Smale complex. The Morse-Smale complex is a decomposition of the domain into regions of similar gradient flow behavior. The gradient of the function f is given by $\nabla f = (\partial_x f, \partial_y f)$. A *gradient line* is a line whose tangent vectors are parallel to the gradient of the function f . For each critical point c we can now define a stable and unstable manifold. The stable manifold is the union of all gradient lines converging to c and the unstable manifold is the union of all integral lines originating from c . If the stable and unstable manifolds only intersect transversally the function f is called *Morse-Smale*. The intersection defines the Morse-Smale complex which segments the domain in the desired way. The complex can be summarized by its skeleton consisting of the critical points and connecting gradient lines also called *separatrices*.

Discrete Morse theory. Morse theory is a topic from differential topology and was originally developed for smooth manifolds and functions. However, the results

from numerical simulations are not a continuous field but discretely sampled data points on a polygonal grid for each time slice. Thus, a direct application of this definition requires the interpolation of the data and the computation of derivatives. This involves many data-specific parameters and is especially challenging when dealing with noisy data. More recently, a discrete version of Morse theory has been introduced by Forman [7]. His theory is purely combinatorial and does not rely on a specific interpolation method and any derivatives. Based on his theory a number of robust topology extraction algorithms for discrete data have been developed.

Forman's theory is based on the notion of *discrete vector fields*. For the definition of discrete vector fields the discrete domain is considered as a simplicial graph. The nodes of the graph consist of the vertices, edges and cells of the domain of mesh. Each node is labeled with the dimension p of the geometric simplex it represents. The links of the graph encode the neighborhood relation of the triangulation.

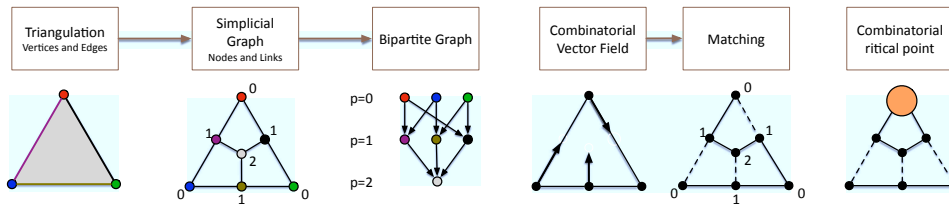


FIG. 13. Basic definitions for a combinatorial vector field

A *combinatorial vector field* V can be defined as a matching of the simplicial graph (see Fig. 13). A matching of a graph is a subset of links such that no two links are adjacent. The nodes of the graph that are not covered by V are called critical points (see Fig. 13, right). The type of a critical point of V is determined by the dimension of the node p . It is called sink if ($p = 0$), saddle if ($p = 1$), or source if ($p = 2$). A combinatorial p -streamline is a path in the graph whose links alternate between V and the complement of V , and the dimension of the nodes of the path alternates between p and $p + 1$. A p -streamline connecting two critical points is called a separatrix. The most important theorems in Morse theory can be transferred to the discrete setting. Due to the finite nature of these definitions, the topological features (critical points, separatrices) can be computed exactly in a combinatorial vector field free of parameters and give very reliable results. For this generation of the discrete gradient field work we use the framework proposed by REINIGHAUS *et al.* [23] together with the ideas from ROBINS *et al.* [25].

References

1. M. BRØNS, B. JAKOBSON, K. NISS, A.V. BISGAARD, L.K. VOIGT, *Streamline topology in the near wake of a circular cylinder at moderate Reynolds numbers*, Journal of Fluid Mechanics, **584**, 23–43, 2007.
2. C. BASDEVANT, T. PHILIPOVITCH, *On the validity of the “Weiss criterion” in two-dimensional turbulence*, Phys. D, **73**, 17–30, 1994.
3. B. CABRAL, L.C. LEEDOM, *Imaging vector fields using line integral convolution*, in: Proceedings of the 20th Annual Conference on Computer Graphics and Interactive Techniques, SIGGRAPH’93, New York, ACM, 263–270, 1993.
4. A.V.G. CAVALIERI, G. DAVILLER, P. COMTE, P. JORDAN, G. TADMOR, Y. GERVAIS, *Using large eddy simulation to explore sound-source mechanisms in jets*, J. Sound Vibr., **330**, 4098–4113, 2011.
5. P. COMTE, J.H. SILVESTRINI, P. BÉGOU, *Streamwise vortices in large-eddy simulations of mixing layer*, Eur. J. Mech. B, **17**, 615–637, 1998.
6. H. EDELSBRUNNER, J. HARER, *Persistent homology — a survey*, in: Surveys on Discrete and Computational Geometry: Twenty Years Later, J. E. Goodman, J. Pach, and R. Pollack, eds., **458**, 257–282, AMS Bookstore, 2008.
7. R. FORMAN, *Morse theory for cell-complexes*, Advances in Mathematics, **134**, 90–145, 1998.
8. J. FREUND, *Noise sources in a low Reynolds number turbulent jet at Mach 0.9*, J. Fluid Mech., **438**, 277–305, 2001.
9. S. GOTO, J.C. VASSILICOS, *Self-similar clustering of inertial particles and zero-acceleration points in fully developed two-dimensional turbulence*, Phys. Fluids, **18**, 115103–1..10, 2006.
10. D. GOTTLIEB, E. TURKEL, *Dissipative two-four methods for time-dependent problems*, Math. of Comp., **30**, 703–723, 1976.
11. G. HALLER, *Distinguished material surfaces and coherent structures in 3D fluid flows*, Physica D: Nonlinear Phenomena, **149**, 248–277, 2001.
12. G. HALLER, *An objective definition of a vortex*, J. Fluid Mech., **525**, 1–26, 2005.
13. F. HAMA, *Streaklines in a perturbed shear flow*, Phys. Fluids, **5**, 644–650, 1962.
14. C. JACKSON, *A finite-element study of the onset of vortex shedding in flow past variously shaped bodies*, J. Fluid Mech., **182**, 23–45, 1987.
15. J. KASTEN, I. HOTZ, B.R. NOACK, H.-C. HEGE, *Vortex merge graphs in two-dimensional unsteady flow fields*, in: Proceedings of Joint EG – IEEE TVCG Symposium on Visualization, 2012.
16. M.J. LIGHTHILL, *Attachment and Separation in Three-Dimensional Flow*, 1st ed., Oxford University Press, Oxford, 1963.
17. J. MILNOR, *Morse Theory*, Princeton University Press, 1963.
18. B.R. NOACK, K. AFANASIEV, M. MORZYN’SKI, G. TADMOR, F. THIELE, *A hierarchy of low-dimensional models for the transient and post-transient cylinder wake*, J. Fluid Mech., **497**, 335–363, 2003.
19. B.R. NOACK, P. PAPAS, P.A. MONKEWITZ, *The need for a pressure-term representation in empirical Galerkin models of incompressible shear flows*, J. Fluid Mech., **523**, 339–365, 2005.

20. B.R. NOACK, I. PELIVAN, G. TADMOR, M. MORZYN'SKI, P. COMTE, *Robust low-dimensional Galerkin models of natural and actuated flows*, in: W. Schröder and P. Tröltzsch, Fourth Aeroacoustics Workshop, Institut für Akustik und Sprachkommunikation, Technische Universität Dresden, 2004.
21. R.W. PANTON, *Incompressible Flow*, Wiley, New York, 1984.
22. A.E. PERRY, M.S. CHONG, *A description of eddying motions and flow patterns using critical-point concepts*, *Ann. Rev. Fluid Mech.*, **19**, 125–155, 1987.
23. J. REININGHAUS, D. GÜNTHER, I. HOTZ, S. PROHASKA, H.-C. HEGE, *TADD: A computational framework for data analysis using discrete Morse theory*, in: Proc. ICMS 2010, 2010.
24. J. REININGHAUS, J. KASTEN, T. WEINKAUF, I. HOTZ, *Efficient computation of combinatorial feature flow fields*, *IEEE Trans. Vis. Comput. Graph.*, **18**, 1563–1573, 2012.
25. V. ROBINS, P. WOOD, A. SHEPPARD, *Theory and algorithms for constructing discrete Morse complexes from grayscale digital images*, *IEEE Transactions on Pattern Analysis and Machine Intelligence*, **33**, 1646–1658, 2011.
26. D. RODRIGUEZ, V. THEOFILIS, *Structural changes of laminar separation bubbles induced by global linear instability*, *J. Fluid Mech.*, **655**, 280–305, 2010.
27. D. RODRIGUEZ, V. THEOFILIS, *On the birth of stall cells on airfoils*, *Theor. Comput. Fluid Dyn.*, **25**, 105–117, 2011.
28. M. SCHUMM, E. BERGER, P. MONKEWITZ, *Self-excited oscillations in the wake of two-dimensional bluff bodies and their control*, *J. Fluid Mech.*, **271**, 17–53, 1994.
29. D. STALLING, H.-C. HEGE, *Fast and resolution independent line integral convolution*, in Proceedings of the 22nd Annual Conference on Computer Graphics and Interactive Techniques, SIGGRAPH'95, New York, NY, USA, 1995, ACM, 249–256, 1995.
30. J. STUART, *On finite amplitude oscillations in laminar mixing layers*, *J. Fluid Mech.*, **29**, 417–440, 1967.
31. G.I. TAYLOR, *The spectrum of turbulence*, Proceedings of the Royal Society of London, Series A, Mathematical and Physical Sciences, **164**, 476–490, 1938.
32. M. TOBAK, D.J. PEAKE, *Topology of three-dimensional separated flows*, *Ann. Rev. Fluid Mech.*, **14**, 61–85, 1982.
33. L. WANG, N. PETERS, *The length-scale distribution function of the distance between extremal points in passive scalar turbulence*, *J. Fluid Mech.*, **554**, 457–475, 2006.
34. L. WANG, N. PETERS, *Length-scale distribution functions and conditional means for various fields in turbulence*, *J. Fluid Mech.*, **608**, 113–138, 2008.
35. C. WILLIAMSON, *Vortex dynamics in the cylinder wake*, *Ann. Rev. Fluid Mech.*, **28**, 477–539, 1996.
36. A. ZEBIB, *Stability of viscous flow past a circular cylinder*, *J. Eng. Math.*, **21**, 155–165, 1987.
37. H.-Q. ZHANG, U. FEY, B.R. NOACK, M. KÖNIG, H. ECKELMANN, *On the transition of the cylinder wake*, *Phys. Fluids*, **7**, 779–795, 1995.

Received August 21, 2015; revised version December 22, 2015.
